Journal of Molecular Modeling (2023) 29:92
https://doi.org/10.1007/s00894-023-05491-x

ORIGINAL PAPER

Possible boron-rich amorphous silicon borides from ab initio simulations

Ayşegül Özlem Çetin Karacaoğlan[1] · Murat Durandurdu[1]

Received: 17 August 2022 / Accepted: 27 February 2023 / Published online: 10 March 2023

Abstract

Context By means of ab initio molecular dynamics simulations, possible boron-rich amorphous silicon borides (B_nSi_{1-n}, $0.5 \leq n \leq 0.95$) are generated and their microstructure, electrical properties and mechanical characters are scrutinized in details. As expected, the mean coordination number of each species increases progressively and more closed packed structures form with increasing B concentration. In all amorphous models, pentagonal pyramid-like configurations are observed and some of which lead to the development of B_{12} and $B_{11}Si$ icosahedrons. It should be noted that the $B_{11}Si$ icosahedron does not form in any crystalline silicon borides. Due to the affinity of B atoms to form cage-like clusters, phase separations (Si:B) are perceived in the most models. All simulated amorphous configurations are a semiconducting material on the basis of GGA+U calculations. The bulk modulus of the computer-generated amorphous compounds is in the range of 90 GPa to 182 GPa. As predictable, the Vickers hardness increases with increasing B content and reaches values of 25-33 GPa at 95% B concentration. Due to their electrical and mechanical properties, these materials might offer some practical applications in semiconductor technologies.

Method The density functional theory (DFT) based ab initio molecular dynamics (AIMD) simulations were used to generate B-rich amorphous configurations.

Keywords Boron-rich · Silicon borides · Amorphous · Ab initio

Introduction

The boron-silicon (BSi) binary compounds have drawn substantial attentions for many years. The existence of these compounds was recognized more than one century ago. However, there are still unknows and controversies about them. The first reports dated back to the study of Moissan and Stocks in 1900s in which silicon triboride (c-SiB_3) and silicon hexaboride (c-SiB_6) were ferreted out in the crystalline form by the technic of fusion of elements [1], but no information was provided about their crystal structure. Later, c-SiB_3, as a single crystal phase having a tetragonal symmetry, was affirmed with the hot-pressing method between 1873 and 2073 K by Samsanov and Latisheva in 1955 [2]. In 1956, Zhuravkev proposed that c-SiB_6 had a structure resembling to the cubic compound of CaB_6 [3]. However, the later investigations on SiB_6 did not validate the cubic crystal, and as an alternative, they proposed an orthorhombic structure [4–8]. The crystalline silicon tetraboride (c-SiB_4), a more well-known B-Si binary compound, was fabricated in different experiments in 1960 [9–11]. Yet, the presence of a cubic form of c-SiB_4 and its quality and impurities were questioned in other studies [12–14]. In spite of a few published data [2, 15, 16], its physical and mechanical properties remained unknown until 1989 at which Tremblay and Angers discovered an interesting and effective technic to produce SiB_4 powders [17] and revealed its physical (porosity, specific density, and microstructural aspects) and mechanical properties (elastic modulus, flexural strength, and Vickers microhardness) in details. [18]. In summary, there are three different types in the phase diagram of B-rich crystal binary compounds, which are referred as c-SiB_3 (and/or SiB_4), c-SiB_6, and c-SiB_n [19].

B-rich molecules or solids have an important significance in physics, chemistry, and materials science due to their remarkable properties. The main characteristic of icosahedral B-rich systems, for example, B_4C, SiB_3, B_6O, and SiB_3

✉ Murat Durandurdu
murat.durandurdu@agu.edu.tr

[1] Nanotechnology Engineering and Materials Science and Mechanical Engineering Program, Abdullah Gül University, Kayseri, Turkey

[20–24], is composed of the α-rhombohedral phase of B (α-B_{12}) and their arrangements [25, 26]. These solids show superb thermoelectric performance and resist to high melting temperatures up to 2400 °C [26]. For this reason, they are referred as very stable refractory materials having high melting temperatures [25]. Moreover, they have a low mass density, splendid hardness, good chemical inertness, adjustable semiconducting aspects, high elasticity modulus, high mechanical strength, and high stability in oxygen [27–30].

Both Si-rich and B-rich noncrystalline solids can be easily synthesized. The first amorphous semiconducting B_nSi_{1-n} ($0 \le n \le 1$) alloys were prepared by the rf (radio frequency) plasma decomposition of SiH_4-B_2H_6 gas mixtures in 1979 [31]. In this research, the infrared vibrational modes, the optical absorption, the electrical conductivity, the spin resonance, and the hydrogen content (between 10 and 45% hydrogen) of these films were analyzed [31]. In 1983, amorphous B-Si alloys with 0–40% B concentrations were generated by low-pressure chemical vapor deposition (LPCVD) technique, and their thermal oxidation was examined [32]. In a different experiment (in 1993), amorphous B_nSi_{1-n} ($0 \le n \le 1$) thin films were easily produced by the LPCVD method as well, and the impacts of Si incorporation on their structural modifications were explored [33]. Si-rich-disordered BSi alloys with 1–50 at. % B were produced by the LPCVD, and the change in optical band gap was studied [34]. A few years later, the same group prepared Si-rich amorphous BSi materials with 0–25 at. % B, and their oxidation at temperatures of 25–600 °C was qualitatively explored [35]. B-rich BSi compounds having 90–97% B contents were fabricated by the arc-melting and spark plasma sintering, and the thermoelectric properties and the effects of phase composition and microstructure on the thermoelectric properties were explored [36]. In the last study, B-rich B-Si films by the pulsed laser deposition (PLD) technique with different B/Si ratios were prepared, and the change in band gap energy was projected from the optical absorption spectrum of the films [37]. The authors deduced an increase in the band gap with decreasing B concentration [37].

According to our literature review, amorphous BSi binary compounds (B_nSi_{1-n}, $0.5 \le n \le 0.95$) are still one of inadequately known B-involving solids as semiconductors and refractory materials because no extensive investigation has been carried out to understand their structure at the atomistic level and their electrical and mechanical properties so far. This paper reports a detailed examination of B-rich amorphous SiB with 50–95 at. % B to provide valuable information about their features.

Computational method

In order to create B-rich amorphous models, the density functional theory (DFT)-based ab initio molecular dynamics (AIMD) simulations were used [38]. The pseudopotentials were due to the Troullier-Martins approach [39]. The DZ basis sets were selected for the valance electrons, and the Γ point was chosen to sample the Brillouin zone. The exchange correlation energy was estimated via the Perdew-Burke-Ernzerhof (PBE)-generalized gradient approximation (GGA) [40]. To execute AIMD simulations, the NPT (i.e., isothermal-isobaric) ensemble was preferred. The velocity scaling method was used to control temperature, and the Parrinello-Rahman technique [41] with the fictitious mass of 20.0 $Ry.fs^2$ was used to control pressure. Periodic boundary conditions were applied in the simulations. In an MD simulation, a small-time step is more desirable to accurately sample highest frequency motion; its typical value is 1.0 fs, and hence, in the current study, this typical value was used. Since 200 atom models are fair enough to capture the short-range order of amorphous networks, we used a 200 atoms-BN melt having almost no chemical disorder as starting structure and contracted our $B_{0.5}Si_{0.5}$ configuration (100 B atoms and 100 Si atoms) by replacing N atoms with Si atoms. Then, B atoms were randomly substituted with Si atoms until the structure reached to certain B contents. In this way, we created ten different configurations ranging from 50 to 95% B contents. Each initial structure was thermalized at a different temperature according to BSi phase diagram [42]. The lowest temperature (1800 K) was applied to 50% B content while the highest one (2300 K) was applied to 95% B content for 30 ps. The melts were then slowly quenched to the room temperature in 75.0–100.0 ps. By using the conjugate gradient method, the final structures at 300 K were optimized such that the greatest forces on atoms are smaller than 0.01 eV/Å. In addition to these amorphous configurations, we also studied c-SiB_3 and c-SiB_4 to compare their features with those of the amorphous models. In order to accurately estimate the band gap energy of the amorphous structures, we performed the GGA+U calculations. In order to evaluate the Hubbard potential U, we focused on the $B_{50}Si_{50}$ model because the band gap was estimated about 0.8 eV for the $B_{50}Si_{50}$ thin film [37]. The Hubbard potentials $U = 8.0$ eV for B-p state and $U = 7.0$ eV for Si-p state were found to produce about 0.8 eV band gap energy for our $B_{50}Si_{50}$ model, and hence, we used these two parameters for all other amorphous configurations to predict their electronic structure. The optimized structures were used for the structural analysis and the estimation of the electirical and mechanical properties.

Results

Atomic structure

The partial pair distribution functions (PPDFs)

First, we probe the amorphous configurations using the partial pair distribution functions (PPDFs) since PPDFs can

offer valuable information about their microstructure. The PPDFs of some models generated are depicted in Fig. 1. All PPDFs exhibit classic characteristics of an amorphous network such that they all show a well-defined short-range correlation but not long-range ones. In order to reveal the influence of B content on the average B-B, B-Si, and Si-Si bond separations, the position of first maximum peak in all correlations is studied and plotted in Fig. 2. The B-B bond length is projected to be in the range of about 1.76–1.77 Å, implying that the change in B/Si composition has almost no effect on this bond length. One might expect to see a cumulative trend in the B-B separation with increasing B concentration because the mean coordination number of B atoms rises with increasing B content (see below). Indeed, B atoms have a strong tendency to form the pentagonal pyramids (B_6) and hence B_{12} molecules. In the amorphous configurations, the B-B bonds mainly involve pentagonal pyramid-like motifs. As B content increased, more pyramid-like units form, and hence, a noticeable change in the B-B separation is not observed. For c-SiB_3 and c-SiB_4, the B-B bond separation is computed to be 1.77 Å and 1.82 Å, respectively.

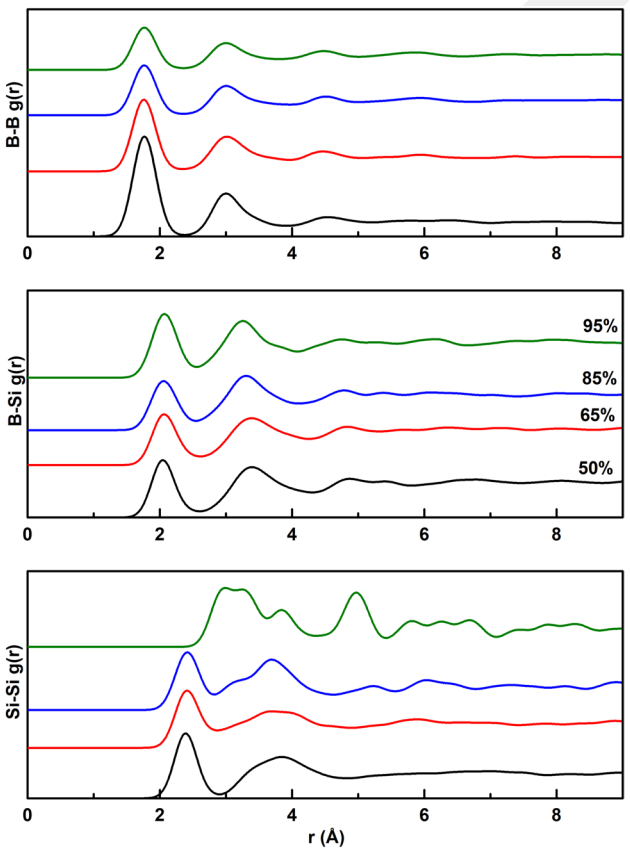

Fig. 1 The partial pair distribution functions (PPDFs) of some computer-generated BSi amorphous models relaxed using the conjugate gradient technique. PPDFs are plotted using a Gaussian smoothing factor of 0.05. It should be noted that Si-Si bonds do not form in a-$B_{95}Si_5$

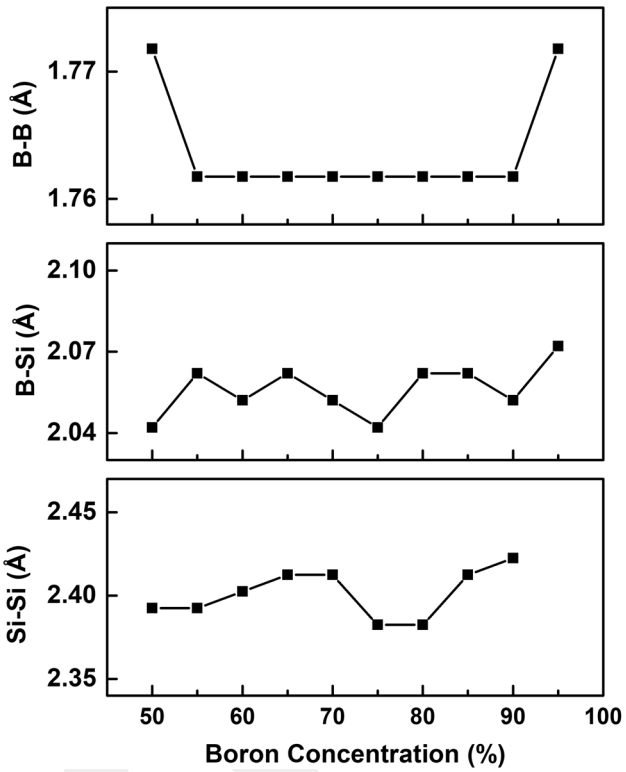

Fig. 2 The computed bond length of B-B, B-Si and Si-Si pairs vs B concentration

When the previous experimental and theoretical studies on the crystalline BSi materials are considered, the estimated range for B-B bond is well-comparable with the values of 1.75–1.90 Å in c-$SiB_{2.5}$ (the monoclinic symmetry) [43], 1.74–1.92 Å in c-SiB_3 (the triclinic symmetry) [43], 1.792 Å in c-SiB_3 (the orthorhombic symmetry) [44], 1.84 Å in c-$B_{2.89}Si$ [12], and 1.77-1.85 Å in c-SiB_6 [8]. The average B-Si bond distance slightly fluctuates between 2.04 and 2.07 Å, again, suggesting no strong influence of B content on this bond length as well. The B-Si bond length is computed to be 1.99 Å for c-SiB_3 and 2.01 Å for c-SiB_4. Our predictions are quite comparable with the earlier experimental and theoretical results of 2.02–2.22 Å in c-$SiB_{2.5}$ (the monoclinic symmetry) [43], 2.00–2.22 Å in c-SiB_3 (the triclinic symmetry) [43], 2.02–2.17 Å in c-SiB_6 [8], and 2.002 Å in c-$B_{2.89}Si$ [12]. As regards to the mean Si-Si bond separation, it is in the range of 2.38 to 2.42 Å. The change in this bond distance, again, is not too drastic. The average Si-Si bond length from our simulation is 2.57 Å for c-SiB_3 and 2.15 Å for c-SiB_4. The Si-Si bond separation obtained in the present work is slightly longer than 2.33 Å in c-$SiB_{2.5}$ (the monoclinic symmetry) [43], 2.36 Å in c-SiB_3 (the triclinic symmetry) [43], 2.12–2.21 Å in c-SiB_6 [8], and 2.35–2.36 Å in c-Si [45]. We should note here that there is no Si-Si bonding at 95% B content, and hence, the peak in the PPDFs around 3 Å corresponds to the second neighbor coordination shell.

The coordination number

The mean coordination numbers are indeed one of the key parameters for amorphous materials. By using the first minimum of PPDFs (2.34–2.37 Å for the B-B pair, 2.54–2.62 Å for the B-Si pair, and 2.82–3.02 Å for the Si-Si pair depending upon B concentration), the coordination numbers are estimated, and their variation as a function of B content is illustrated in Fig. 3. The trend in B and Si coordination is similar, and they increase with increasing B/Si composition. The coordination for B atom changes from 5.49 to 6.18 while that of Si atom changes from 4.29 to 5.6 with increasing B content. We should note that the value of 6.18 for B atom is comparable with 6.3 in amorphous B [25]. We also note here that the mean coordination number of B atom in amorphous SiB_3 and SiB_4, about 5.8, is comparable with 6 in their crystalline counterpart. Additionally, the average coordination number (about 4.6) of Si atom in a-SiB_3 is close to 5.0 in c-SiB_3 while the noticeable deviation in Si coordination (4.7) is observed in the amorphous SiB_4 phase, compared to 3.3 in c-SiB_4. It should be noted here that the coordination numbers estimated depend on the cutoff distances used, and hence, we do expect some minor errors in these coordination numbers (Fig. 3).

As seen from Fig. 4 at 50% B content, the structure consists of mainly fourfold coordinated Si atoms (77.0%) and sixfold coordinated B atoms (56.0%). The fraction of fivefold and sixfold coordinated Si atoms is ~12% and 8%, correspondingly. These higher coordinated Si atoms mainly involve pentagonal-like configurations. On the other hand, the frequency of fourfold and fivefold coordinated B atoms is about 16.0% and 22.0%, respectively. The tetrahedral coordination of B and Si atoms decreases with increasing B/Si composition, but it does not diminish even at the highest B concentration. Parallel to this decrease, the fraction of 5- and 6-fold coordinated motifs for Si atom increases gradually whilst fivefold coordination for B atoms decreases. Some models also present negligible amount of 3-fold and 8-fold coordinated Si atoms.

The bond angle distribution

In order to shed additional lights onto the atomic structure of amorphous B_nSi_{1-n} configurations, a bond angle distribution examination is carried out, and the B-B-B, B-Si-B, Si-B-Si, and Si-Si-Si distributions are illustrated in Fig. 5. There are two main peaks located at ~60° and ~108° related to the B-B-B angles for all compositions, which are a result of the intra-icosahedral bonds of the pentagonal pyramids

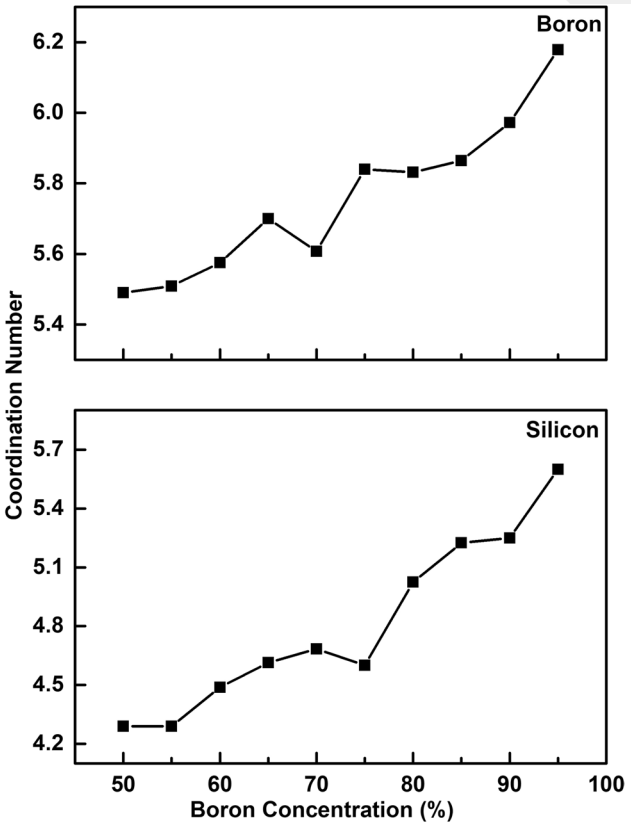

Fig. 3 B content dependence of average coordination number of B and Si atoms

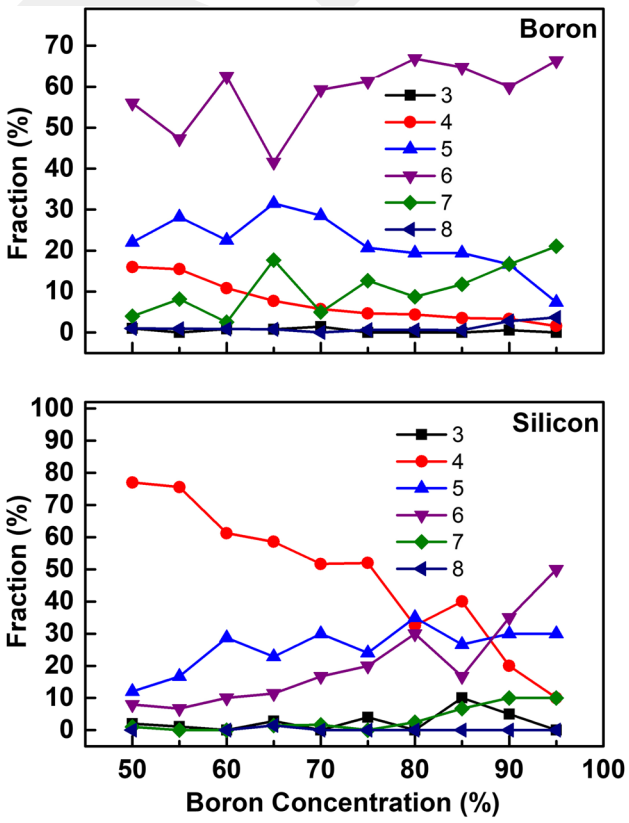

Fig. 4 The coordination distributions of B and Si atoms as a function of B concentrations

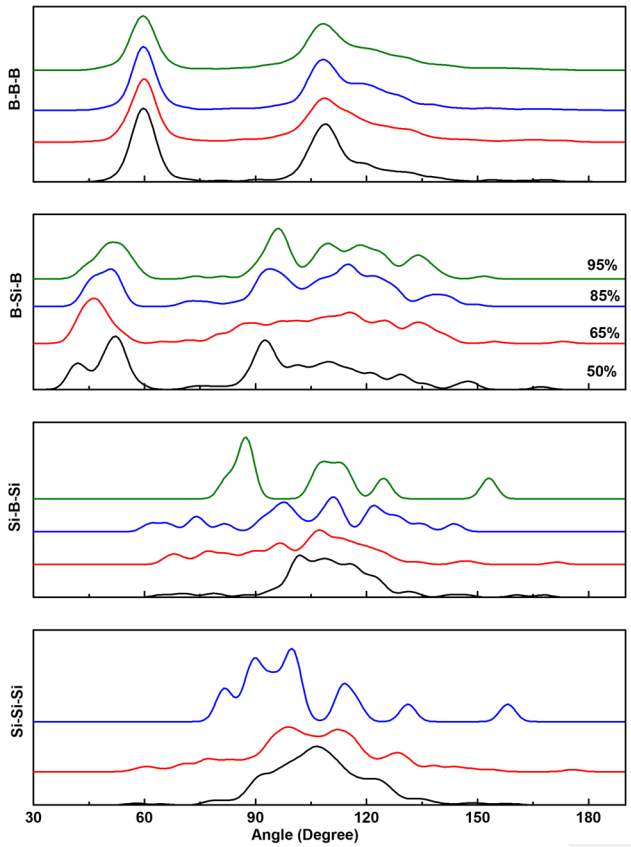

Fig. 5 The bond angle distribution function (BADF) of some amorphous configurations relaxed using the conjugate gradient technique. BADFs are plotted using a smoothing factor of 4°

(i.e., B_{12} molecules), similar to those of pure amorphous or crystalline B structures. For the Si-B-Si angle distributions, a broad peak located around 111°, close to the tetrahedral angle of 109.5° up to 80% B content, suggests some signature of tetrahedral character in these amorphous networks. Yet, beyond 80% B content, this character diminishes due to the formation of higher coordinated motifs around Si-atoms. Indeed, the Si-Si-Si angle distribution also shows similar trend as in the Si-B-Si distribution. B-Si-B angles, on the other hand, produce the most complex distribution because of differently coordinated Si atoms involving both tetrahedral and pentagonal pyramid-like motifs.

The Voronoi analysis

The Voronoi polyhedron investigation [46, 47] can offer useful information regarding the types of clusters formed around each atom and hence about the amorphous models. In this method, a polyhedron is indicated in the way of $<n_3, n_4, n_5, n_6, \ldots>$ type indices. In here, n_i and Σn_i are the number of i-edge faces of a polyhedron and its total coordination number, correspondingly. In order to identify Voronoi polyhedrons, the first minimum of PPDFs was used as a cutoff radius. The key structure of amorphous and crystalline B and B-rich materials is mostly the quasi-molecular B_{12} icosahedrons formed by the pentagonal pyramids. In the Voronoi analysis, the pentagonal pyramid-like motifs can be represented by <2,2,2,0> index. In B-based amorphous materials, incomplete pentagonal pyramid-like clusters can also form and can be denoted by <2,3,0,0> index. Therefore, we mainly focus on these two indices and analyze their variation (Fig. 6). With reference to B atoms, the fraction of <2,2,2,0> type polyhedrons increases gradually with increasing B content as expected, and parallel to this increase, the frequency of <2,3,0,0> type index decreases slowly, but they still exist at the highest B content and have a fraction of ~7%.

The computer-generated models are visualized via the VESTA program [48], and the models are shown in Fig. 7. By means of Voronoi analyses and visualizations, we observe the formation of the complete B_{12} and $B_{11}Si$ icosahedrons (see Fig. 8) and the development of B_{10}, B_{13}, and B_{14} molecules in some models.

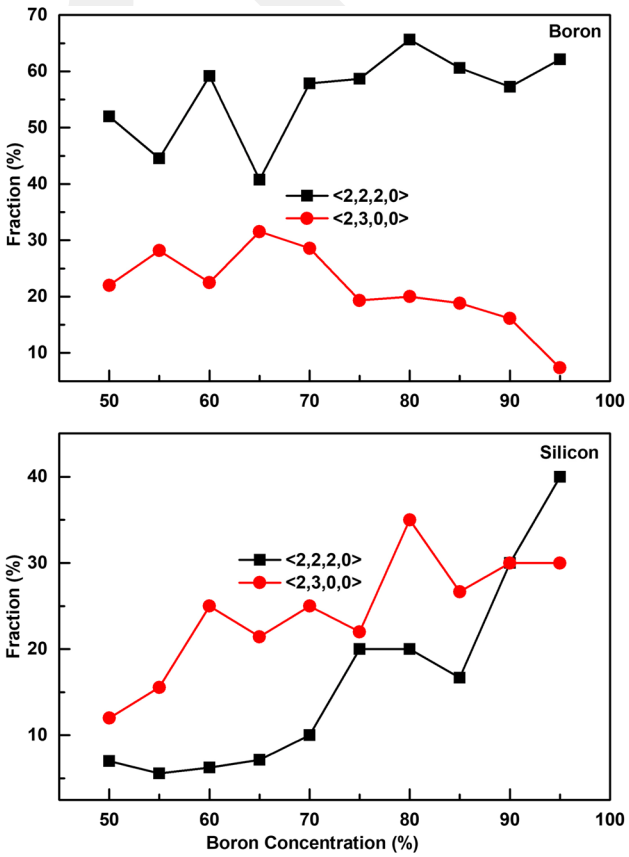

Fig. 6 B content dependence of <2,2,2,0> and <2,3,0,0> indices that correspond to ideal and incomplete pentagonal pyramid-like motifs, respectively

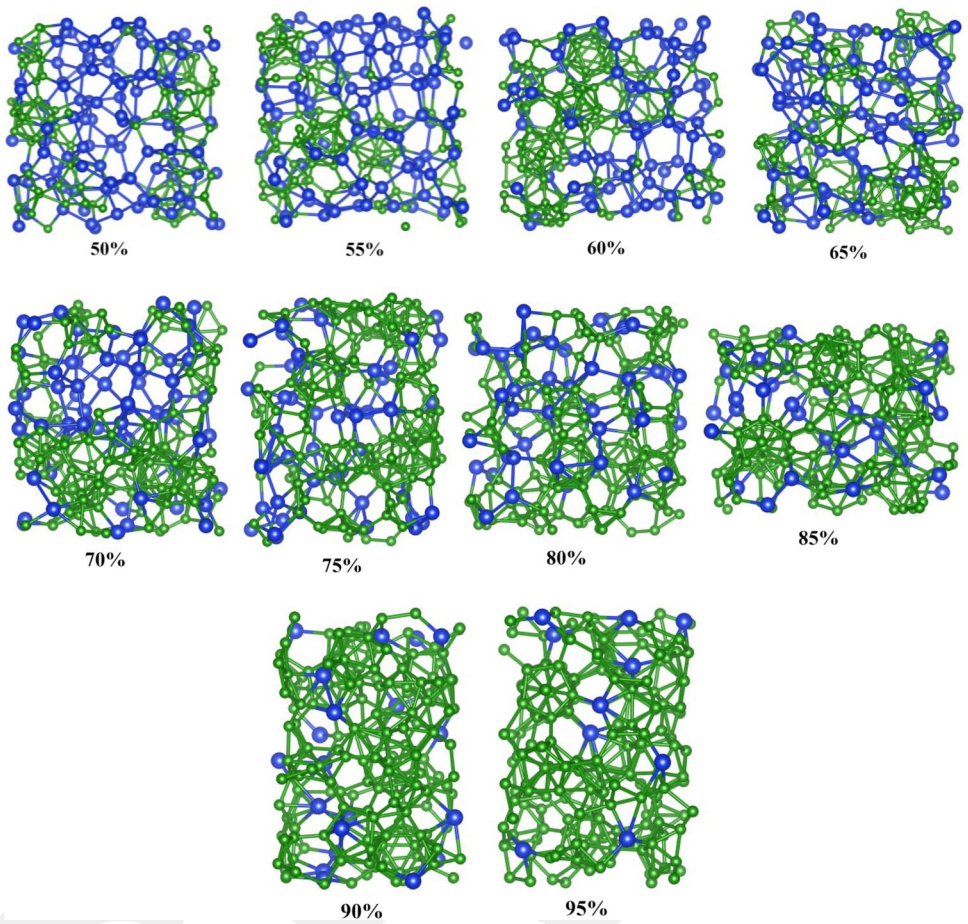

Fig. 7 Ball-stick representation of modeled noncrystalline configurations

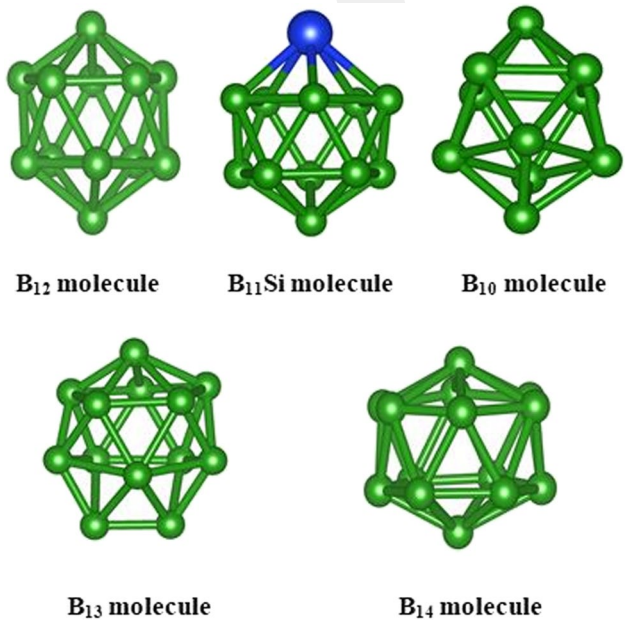

Fig. 8 Cage-like clusters formed in the amorphous BSi systems

The electronic properties

The amorphous and crystalline BSi materials can have important technological applications, in particular in the semiconducting technology. For this reason, determining their

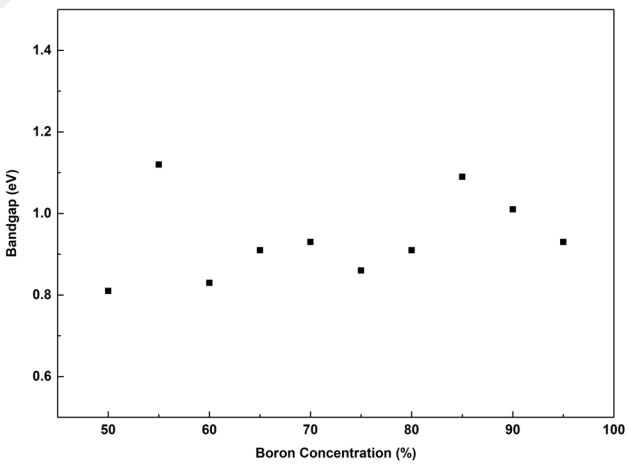

Fig. 9 B content dependence of forbidden energy band gap based on GGA+U calculations

electronic structure is essential. Figure 9 depicts the variation of HOMO-LUMO band gap energy predicted using GGA+U calculations as a function of B content. The band gap does not show a clear trend but fluctuates between 0.81 and 1.12 eV, comparable with 0.5–1.0 eV reported for B:Si thin films [37].

The mechanical properties

For the functional applications of a material, it is necessary to identify its mechanical characteristics. For this reason, we consider the mechanical features of each amorphous configuration in details. We first probe the bulk modulus (K) that can be readily calculated by fitting the energy (E)-volume (V) correlation (Fig. 10) to the third-order Birch-Murnaghan equation of states:

$$E(V) = E_o + \frac{9V_O K}{16}\left\{\left[\left(\frac{V_O}{V}\right)^{\frac{2}{3}} - 1\right]^3 K' + \left[\left(\frac{V_O}{V}\right)^{\frac{2}{3}} - 1\right]^2\left[6 - 4\left(\frac{V_O}{V}\right)^{\frac{2}{3}}\right]\right\} \quad (1)$$

where $K' = dK/dP$ (P is pressure) and the subscript "0" represents the equilibrium values. The computed K values as a function of B concentration are illustrated in Fig. 11 and given in Table 1 as well. For comparison,

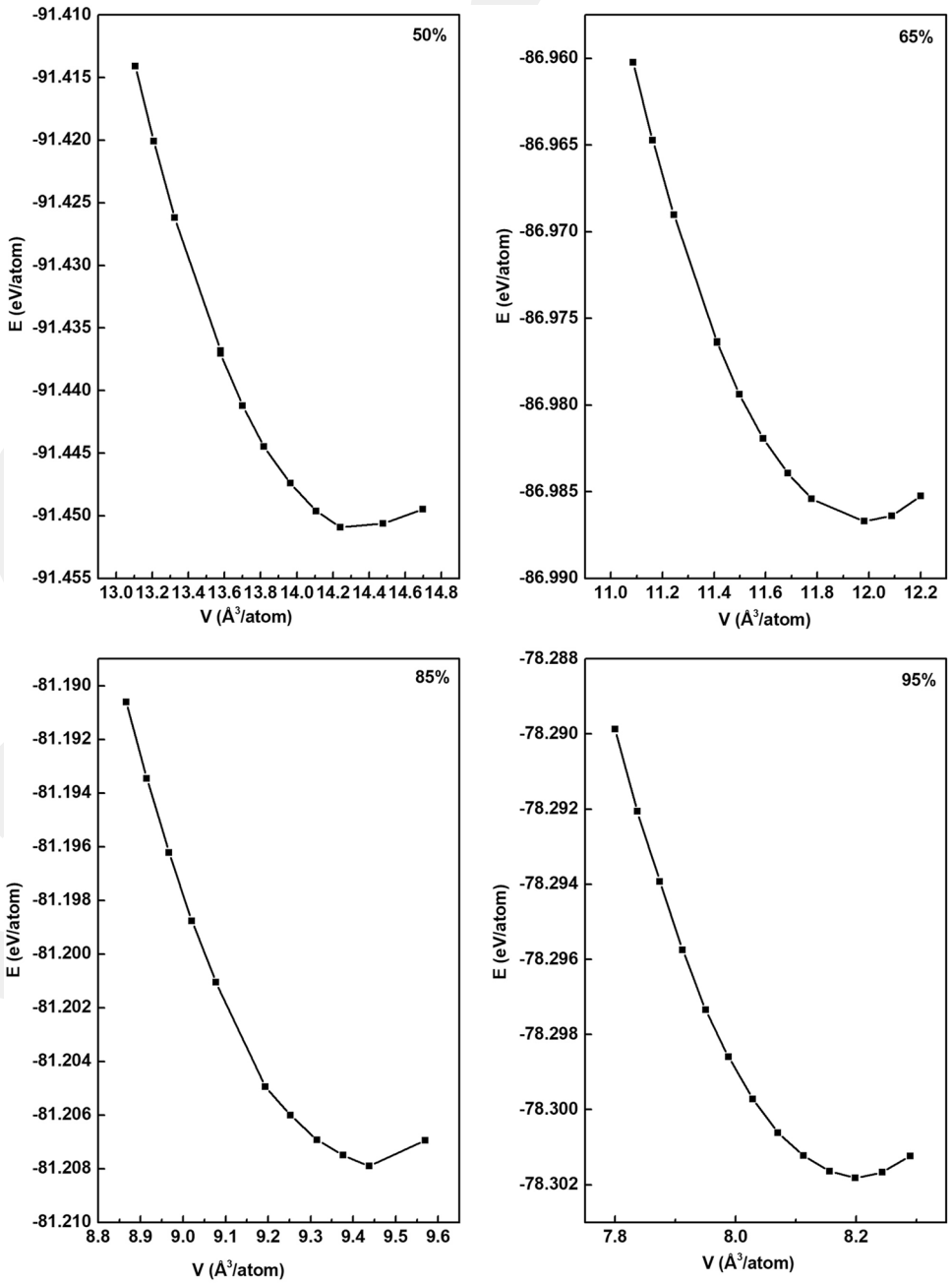

Fig. 10 Energy-volume relation of some BSi amorphous models

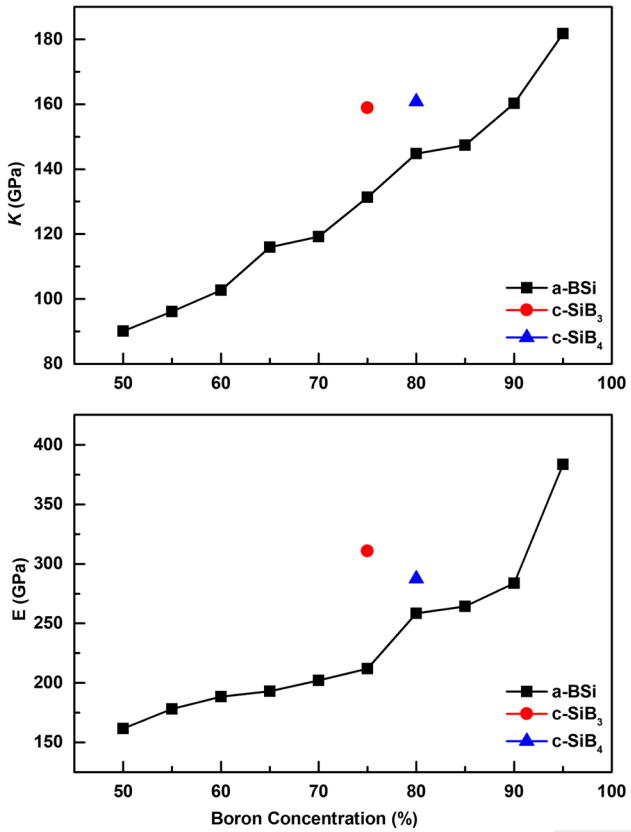

Fig. 11 Change in bulk (*K*) and Young (*E*) moduli as a function of B concentration

available data in the literature are also provided in the same table. The *K* value of the amorphous materials drastically changes from ~90 to ~182 GPa with increasing B content, as expected to due to the formation of more B_{12} molecules in the system. The bulk modulus of c-SiB_3 and c-SiB_4 is also computed and found to be ~159 GPa and ~161 GPa, respectively, which are approximately overlapped with the earlier theoretical results of about 121.1–183.5 GPa for c-SiB_3, c-SiB_4, c-SiB_6, and c-SiB_{36} [50]. For the amorphous form of c-SiB_3 and c-SiB_4, a slight reduction in *K* value (see Table 1) is observed due to their disordered nature. It should be noted here that the computed bulk modulus of the amorphous materials with high B contents seems to be reasonably comparable with that of pure B crystals (α-, β-, γ-, and tetragonal forms) having $K \approx 200$ GPa [49, 51–53].

In order to predict Young modulus (*E*), a uniaxial stress along the principal axes of the modeled amorphous materials and the crystalline phases is applied, and their atomic coordinates are relaxed. Then, the stress-strain relation is studied and from the slope of the relation, Young modulus (*E*)

$$E = -\frac{\sigma_{axial}}{\varepsilon_{axial}} \tag{2}$$

is obtained and depicted in Fig. 11. Young modulus increases from ~162 to 384 GPa with increasing B content, indicating that the materials become less elastic at high B contents. Young modulus of c-SiB_3 and c-SiB_4 is calculated as ~311 GPa and ~288 GPa, respectively. The estimated values are, as seen in Table 1, parallel to the results of ~150–359 GPa in c-SiB_3, c-SiB_6, and c-SiB_{36} [50].

Knowing *E* and *K* allows us to calculate Poisson ratio (ν) using the following equation:

$$\nu = \frac{1}{2} - \frac{E}{6K} \tag{3}$$

As seen from Fig. 12, ν shows a fluctuant tendency (~0.19–0.23) up to 90% at B, and then, it drastically decreases to ~0.15 at 95% B ratio. ν is estimated to be 0.17 for c- SiB_3 and 0.2 for c-SiB_4. From Table 1, it can be seen that the estimated values of ν for the crystalline and amorphous structures are coherent with 0.17–0.35 in c-SiB_3, c-SiB_6, and c-SiB_{36} [50, 54]. Additionally, the value (0.148) is quite close to 0.11–0.13 in B crystals [52, 53, 55].

Since we acquire *E* and ν values, shear modulus (μ) can be easily computed as

$$\mu = \frac{E}{2(1+\nu)} \tag{4}$$

Shear modulus of the simulated amorphous models possesses a steady increase from ~67 to 167 GPa (see Fig. 12) with increasing B content. We estimate μ to be ~132 GPa for c-SiB_3 and ~120 GPa for c-SiB_4. The calculated values are again close to ~55–154 GPa reported for B-rich BSi crystals [49]. On the other hand, the maximum value is noticeably less than ~197–236 GPa in the crystalline B phases [52–54]. The smaller result in the amorphous forms signifies that they have more flexible structure than the crystalline forms.

In addition to these mechanical parameters, we finally evaluate the Vickers hardness (H) using the next three empirical equations [56–58]:

$$H = 0.151\mu \tag{5}$$

$$H = 2\left(\frac{\mu}{n^2}\right)^{0.585} - 3(\text{GPa}) \tag{6}$$

and

$$H = 0.92\left(\frac{1}{n}\right)^{1.137}(\mu)^{0.708} \tag{7}$$

The results obtained from these equations are given in Fig. 13. The hardness shows an undulate trend but a sudden jump at 95% B concentration. The computed *H* value for our

Table 1 Bulk (K), Young (E) and shear (μ) moduli, Poisson ratios (ν), Pugh's ratio (n), and Vicker's hardness (H). *K*, *E*, μ, and *H* are in the unit of GPa

Phase	*K*	*E*	*ν*	μ	*n*	References
a-$B_{50}Si_{50}$	90.1	161.6	0.2	67.3	1.339	This study
a-$B_{55}Si_{45}$	96.1	178.1	0.191	74.8	1.285	This study
a-$B_{60}Si_{40}$	102.7	188.5	0.194	78.9	1.301	This study
a-$B_{65}Si_{35}$	115.9	192.9	0.223	78.9	1.469	This study
a-$B_{70}Si_{30}$	119.2	201.9	0.217	82.9	1.436	This study
a-$B_{75}Si_{25}$	131.4	211.8	0.231	86.0	1.528	This study
a-$B_{80}Si_{20}$	144.8	258.5	0.203	107.5	1.348	This study
a-$B_{85}Si_{15}$	147.4	264.3	0.201	110	1.339	This study
a-$B_{90}Si_{10}$	160.3	283.7	0.205	117.7	1.362	This study
a-$B_{95}Si_{5}$	181.8	383.6	0.148	167	1.089	This study
c-$B_{75}Si_{25}$	159	310.8	0.17	132.4	1.2	This study
c-$B_{80}Si_{20}$	161	288	0.214	119.6		This study
c-SiB_3	171.2	310.8	0.20	129.8	1.32	[47]
c-SiB_4		280				[16]
		138.4–339.8				[18]
	172.1	150	0.35	55.4	3.11	[47]
c-SiB_6	179.2	358.8	0.17	153.8	1.17	[47]
	81.24					[49]
c-SiB_6-81	121.1	163.8	0.27	64.3	1.88	[47]
c-SiB_{36}	183.5	358.1	0.17	152.4	1.20	[47]
c-Boron	185–231.5					[37, 48, 50, 51]
		445–550	0.11–0.13	197–236		[50–52]

Ref. 16—experiment
Ref. 18—experiment (in different densities)
Ref. 47—theory
Ref. 48—theory
Ref. 49—experiment
Ref. 50—theory
Ref. 51—theory
Ref. 52—theory-diamond-like
Ref. 53—experiment

B-rich-disordered configurations is estimated to be in the range of 10 to 33 GPa. Additionally, the *H* value for c-SiB_3 and c-SiB_4 is computed to be 20–25 GPa and 18.1–20.2 GPa, respectively. Our estimations are in an excellent agreement with the previous experimental and theoretical results of 23–27 GPa estimated for the crystals (23–27 GPa) [16, 18]. Yet the maximum hardness predicted is noticeably less than 42–50 GPa reported for B crystals [59, 60].

The brittle-ductile characteristic of any solid can be classified by means of either the Pugh's ratio (*n*) or Poisson's ratio [61, 62]. The critical value is equal to 1.75 for *n*. If *n* is bigger than 1.75, a solid shows the ductile character. Otherwise, $n < 1.75$, the solid exhibits the brittle character. In addition, if the Poisson ratio is bigger than 0.26, a solid is ductile, and if not, it shows brittle feature [61, 62]. *n* and *ν* values for our B-rich amorphous BSi systems are estimated to be in the range of 1.09–1.53 and 0.191–0.231, respectively, so one can clearly say that our configurations demonstrate a brittle character as it should be in ceramic materials.

Discussion

The B_{12} molecule is the main building unit of B phases and B-rich materials and are observed in all compositions including $B_{50}Si_{50}$ in the present work. This might not be surprising because an experimental investigation reported that a low B content about 17% is enough for the development of B_{12} icosahedra in BSi materials. The present investigation reveals an outstanding feature of B-rich amorphous BSi solids, namely, the formation of ideal $B_{11}Si$ icosahedron(s) in addition to B_{12} molecules in all amorphous structures.

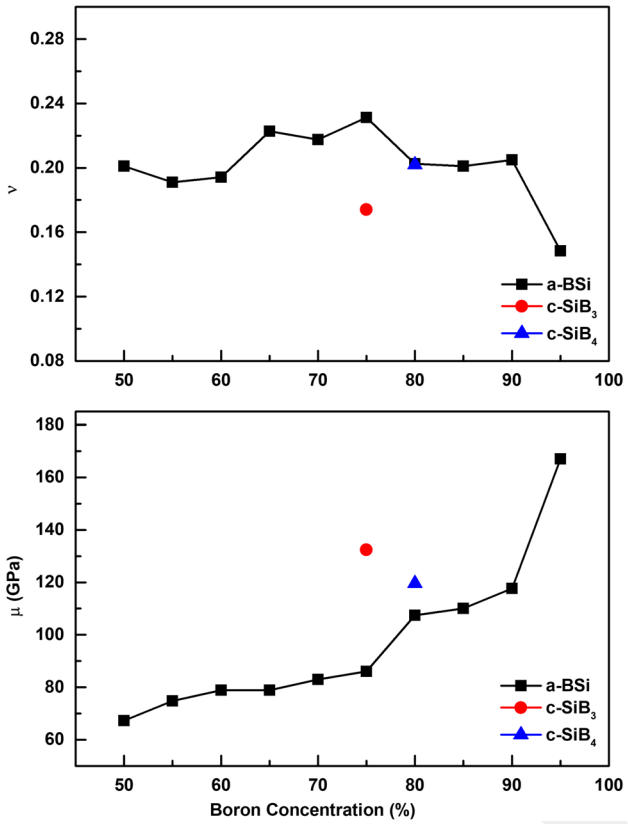

Fig. 12 Variation in Poisson's ration (ν) and shear modulus (μ) vs B content

The ideal $B_{11}Si$ icosahedron does not form in any crystalline BSi phases. The development of ideal $B_{11}Si$ molecules or pentagonal pyramid-like motifs around Si atoms leads to higher mean coordination for Si atoms and a different local arrangement around them in the amorphous configurations compared to the crystals. It should be noted that $B_{11}C$ molecules (in which C atom is sixfold coordinated) do exist in the amorphous and crystalline forms of B_4C, and hence, the observation of high coordinated Si in the amorphous models is unsurprising.

It appears that B atoms have a strong affinity to form pentagonal pyramid-like topologies. This results in B-rich and Si-rich regions in all amorphous models except $B_{95}Si_5$, namely, the occurrence of B:Si phase separations in these amorphous configurations.

We observe the formation of some uncommon cage-like clusters such as B_{10}, B_{13}, and B_{14} in some amorphous network. The B_{10} molecule was perceived in an amorphous BAs model. The others, on the other hand, have not been reported in any B-based materials. Since we did not observe the formation of these unusual molecules in our previous simulations on pure amorphous B, we think that the phase separation (B:Si) provides a driving force of their formation in amorphous BSi materials. Yet, further theoretical studies on a large system, probably using a machine learning potential, are necessary to clarify this matter.

With increasing B content, as a result of the formation of more pentagonal pyramids and hence B_{12} molecules, the mechanical properties of BSi systems are drastically improved, and at high B contents, some mechanical properties of amorphous BSi become comparable with those of B crystals. Consequently, the modeled amorphous materials can be categorized as hard materials because their Vickers hardness is greater than 20 GPa.

Lastly, when the electronic behavior is considered, all amorphous networks show a semiconducting behavior. Subsequently, they can serve as thermoelectric materials and can substitute the crystalline materials that cannot be easily synthesized. Easy production of amorphous materials might provide some advantages over crystalline phases fabricated at certain stoichiometries.

Conclusions

Amorphous B_nSi_{1-n} ($0.5 \leq n \leq 0.95$) configurations are generated by using AIMD simulations, and their local structure, electronic properties, and mechanical features have been investigated and compared with the available data in the literature. The changing B/Si content has almost no effect on the mean bond lengths, but the average coordination number changes from 5.5 to 6.2 for B atoms and from 4.3 to 5.6 for Si atoms. The strong tendency of B atoms to arrange themselves in pentagonal pyramid-like configurations yields Si:B phase separations in the amorphous networks. Most pentagonal pyramid-like motifs lead to the formation of B_{12} and $B_{11}Si$ molecules. The $B_{11}Si$ icosahedrons do not exist in any SiB crystalline phases. The formation of $B_{11}Si$ icosahedrons yields a different local structure in amorphous

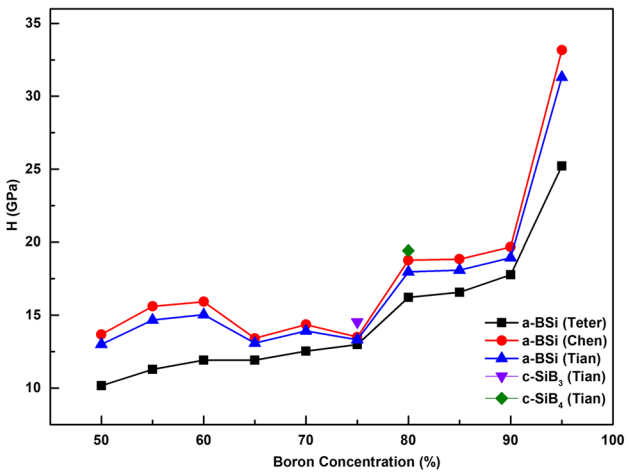

Fig. 13 B concentration dependence of Vickers hardness (H)

configurations, relative to the crystals. When the electronic behavior is discussed, all amorphous compositions can be classified as semiconducting materials having a band gap energy of 0.81–1.12 eV. The bulk modulus of B-rich amorphous silicon borides is calculated to be in the range of ~90 to 182 GPa. The Vickers hardness increases with increasing B content and reaches values of 25–33 GPa at 95% B concentration. Due to their electrical and mechanical properties, these materials can be potential candidates for refractory materials and can substitute the crystalline phases that cannot easily be fabricated.

Acknowledgements The authors are thankful to the Scientific and Technological Research Council of Turkey (TÜBİTAK) under MAG award 117M372. AÖK acknowledges partial financial support from YÖK 100/2000 and TÜBİTAK BİDEB 2211-C programs. We acknowledge the computing time provided by the TÜBİTAK High Performance and Grid Computing Center (TRUBA resources).

Author contribution Ayşegül Özlem Çetin Karacaoğlan: investigation, validation, formal analysis, data curation, writing—original draft, and visualization. Murat Durandurdu: conceptualization, methodology, resources, supervision, funding acquisition, and writing—review and editing.

Data availability The raw/processed data required to reproduce these findings cannot be shared at this time as the data also forms a part of an ongoing study.

Declarations

Competing interests The authors declare no known competing interests.

References

1. Moissan H, Stock A (1990) Preparation and properties of two silicon borides: SiB3 and SiB6. CR Acad Sci 131:139–143
2. Samsonov GV, Latysheva VP (1995) voprosu o khimicheskikh soedineniyakh bora s kremniem. Dokl Akad Nauk SSSR 105:499–499
3. Zhuravlev NN (1956) X-ray determination of the structure of SiB. Kristallografiya 1:666–668
4. Adamsky RF (1958) Unit cell and space group of orthorhombic SiB6. Acta Crystallogr 11:744–745
5. Cline CF (1958) Preliminary investigations of the silicon boride, SiB6. Nature 181:476–477
6. Cline CF (1959) An investigation of the compound silicon boride (SiB6). J Electrochem Soc 106:322–322
7. Giese R (1970) Polyhedral groups in the phase SiB6. Electron Technol 3:151–157
8. Vlasse M, Slack GA, Garbauslas M, Kasper JS, Viala JC (1986) The crystal structure of SiB6. J Solid State Chem 63:31–45
9. Brosset C (1960) Magnusson B. The silicon-boron system. Nature 187:54–55
10. Cline CF, Sands DE (1960) A new silicon boride, SiB4. Nature 185:456–456
11. Matkovich VI (1960) A new form of boron silicide, B4Si. Acta Crystallogr 13:679–680
12. Magnusson B, Brosset C (1962) The crystal structure of B2.8Si. Acta Chem Scand 16:449–455
13. Dietze W, Miller M, Amberger E (1970) Pyrolitic formation of Si-doped B and silicon borides. Electron Technol 3:73–79
14. Rizzo HF, Bidwell LR (1960) Formation and structure of SiB4. J Am Ceram Soc 43:550–552
15. Samsonov GV, Sleptsov VM (1964) Preparation of boron-silicon alloys. Sov Powder Metall Met Ceram 3:488–496
16. Bairamashvili IA, Kalandadze GI, Eristavi AM, Jobava JS, Chotulidi VV, Saloev YI (1979) An investigation of the physicomechanical properties of B6O and SiB4. J Less Common Met 67:455–459
17. Tremblay R (1989) Angers R. Preparation of high purity SiB4 by solid-state reaction between Si and B. Ceram Int 15:73–78
18. Tremblay R, Angers R (1991) Mechanical characterization of dense silicon tetraboride (SiB4). Ceram Int 18:113–117
19. Emin D (1987) Icosahedral boron-rich solids as refractory semiconductors. MRS OPL Archive 97:3–15
20. Lundstro T, Andreev YG (1996) Superhard boron-rich borides and studies of the BCN system. Mater Sci Eng A 209:16–22
21. Slack GA, Morgan KE (2014) Some crystallography, chemistry, physics, and thermodynamics of B12O2, B12P2, B12As2, and related alpha-boron type crystals. J Phys Chem Solid 75:1054–1074
22. Slack GA, McNelly TF, Taft EA (1983) Melt growth and properties of B6P crystals. J Phys Chem Solid 44:1009–1013
23. Hubert H, Devouard B, Garvie LA, O'Keeffe M, Buseck PR, Petuskey WT, McMillan PF (1998) Icosahedral packing of B12 icosahedra in boron suboxide (B6O). Nature 391:376–378
24. Zhang H, Yao S, Widom M (2016) Predicted phase diagram of boron-carbon-nitrogen. Phys Rev B 93:144107
25. Franz R, Werheit H (1991) Boron—rich solids. AIP Conf Proc 231:29
26. Emin D (1987) Icosahedral boron-rich solids. Phys Today 40:55–62
27. Hori A, Takeda M, Yamashita H, Kimura K (1995) Absorption edge spectra of boron-rich amorphous films constructed with icosahedral cluster. J Physical Soc Japan 64:3496–3505
28. Berezin AA, Golokova OA, Kazanin MM, Khomidov T, Mirlin DN, Petrov AV, Umarov AS, Zaitsev VK (1974) Electrical and optical properties of amorphous boron and amorphous concept for ß-rhombohedral boron. J Non Cryst Solids 16:237–246
29. Matsuda H, Nakayama T, Kimura K, Murakami Y, Suematsu H, Kobayashi M, Higashi I (1995) Structural and electronic properties of Li- and Cu-doped β-rhombohedral boron constructed from icosahedral and truncated icosahedral clusters. Phys Rev B 52:6102–6110
30. Motozima S, Sugiyama K, Takahashi Y (1975) Chemical vapor deposition of tetraboron silicide whiskers. Bull Chem Soc Jpn 48:1463–1466
31. Tsai CC (1979) Characterization of amorphous semiconducting silicon-boron alloys prepared by plasma decomposition. Phys Rev B 19:2041–2055
32. Murase K, Ogino T, Mizushima Y (1983) Thermal oxidation of amorphous silicon-germanium-boron alloy. Jpn J Appl Phys 22:1771–1777
33. Ong CW, Chik KP, Wong HK (1993) Effects of Si incorporation on the structural change of a-BxSi1−x alloy films. J Appl Phys 74:6094–6099
34. Yang GR, Zhao YP, Tong BY (1996) FTIR and UV study of amorphous silicon-boron alloys deposited by LPCVD. MRS OPL Archive 426:83–88
35. Yang GR, Zhao YP, Abburi M, Dabral S, Tong BY (1997) Comparison of low-temperature oxidation of crystalline Si and B with a-Si:B alloy: an x-ray photoelectron spectroscopy study. J Vac Sci Technol A 15:279–283
36. Chen L, Goto T, Li J, Hirai T (1996) Synthesis and thermoelectric properties of boron-rich silicon borides. Mater Trans JIM 37:1182–1185
37. Takeda M, Ichimura M, Yamaguchi H, Sakairi Y, Kimura K (2000) Preparation of boron–silicon thin film by pulsed laser deposition and its properties. J Solid State Chem 154:141–144

38. Ordejón P, Artacho E, Soler JM (1996) Self-consistent order-N density-functional calculations for very large systems. Phys Rev B 53:R10441–R10444
39. Troullier N, Martins JL (1991) Efficient pseudopotentials for plane-wave calculations. Phys Rev B 43:1993–2006
40. Perdew JP, Burke K, Ernzerhof M (1996) Generalized gradient approximation made simple. Phys Rev Lett 77:3865–3868
41. Parrinello M, Rahman A (1981) Polymorphic transitions in single crystals: a new molecular dynamics method. J Appl Phys 52:7182–7190
42. Mostafa A, Medraj M (2017) Binary phase diagrams and thermodynamic properties of silicon and essential doping elements (Al, As, B, Bi, Ga, In, N, P, Sb and Tl). Materials 10(6):676
43. Eklöf D, Fischer A, Ektarawong A et al (2019) Mysterious SiB3: identifying the relation between α-and β-SiB3. ACS Omega 4:18741–18759
44. Salvador JR, Bilc D, Mahanti SD, Kanatzidis MG (2003) Stabilization of β-SiB3 from liquid Ga: a boron-rich binary semiconductor resistant to high-temperature air oxidation. Angew Chem 42:1973–1976
45. Gali A, Miro J, Deák P, Ewels CP, Jones R (1996) Theoretical studies on nitrogen-oxygen complexes in silicon. J Phys Condens Matter 8:7711–7722
46. Voronoi G (1908) Recherches sur les paralléloèdres primitives. J Reine Angew Math 134:198–287
47. Brostow W et al (1998) Voronoi polyhedra and Delaunay simplexes in the structural analysis of molecular-dynamics-simulated materials. Physical Review B 57:13448
48. Momma K, Izumi F (2011) VESTA 3 for three-dimensional visualization of crystal, volumetric and morphology data. J Appl Cryst 44:1272–1276
49. Nelmes RJ, Loveday JS, Allan DR, Besson JM, Hamel G, Grima P, Hull S (1993) Neutron-and x-ray-diffraction measurements of the bulk modulus of boron. Phys Rev B 47:7668–7673
50. Zhang B, Wu L, Li Z (2017) Predicted structural evolution and detailed insight into configuration correlation, mechanical properties of silicon–boron binary compounds. RSC Adv 7:16109–16118
51. Zarechnaya EY, Dubrovinsky L, Dubrovinskaia N et al (2009) Superhard semiconducting optically transparent high pressure phase of boron. Phys Rev Lett 102:185501
52. Jiang C, Lin Z, Zhang J, Zhao Y (2009) First-principles prediction of mechanical properties of gamma-boron. Appl Phys Lett 94:191906
53. Aydin S, Simsek M (2011) First-principles calculations of elemental crystalline boron phases under high pressure: Orthorhombic B28 and tetragonal B48. J Alloys Compd 509:5219–5229
54. Getmanskii IV, Minyaev RM, Koval VV, Minkin VI (2018) Quantum chemical modeling of solid-state B4X structures containing tetrahedral B4 units with X= B, C, Al, Si. Mendeleev Comm 28:173–175
55. Qin J, Nishiyama N, Ohfuji H, Shinmei T, Lei L, He D, Irifune T (2012) Polycrystalline γ-boron: as hard as polycrystalline cubic boron nitride. Scr Mater 67:257–260
56. Teter DM (1998) Computational alchemy: the search for new superhard materials. MRS Bull 23:22–27
57. Chen XQ, Niu H, Li D, Li Y (2011) Modeling hardness of polycrystalline materials and bulk metallic glasses. Intermetallics 19:1275–1281
58. Tian Y, Xu B, Zhao Z (2012) Microscopic theory of hardness and design of novel superhard crystals. Int J Refract Met Hard Mater 33:93–106
59. Oganov AR, Chen J, Gatti C et al (2012) Ionic high-pressure form of elemental boron. Nature 457:863–867
60. Solozhenko VL, Kurakevych OO, Oganov AR (2008) On the hardness of a new boron phase, orthorhombic γ-B28. J Superhard Mater 30:428–429
61. Vaitheeswaran G, Kanchana V, Svane A, Delin A (2007) Elastic properties of MgCNi3—a superconducting perovskite. J Phys Condens Matter 19:326214
62. Frantsevich IN (1982) Elastic moduli of metals and ınsulators handbook. Naukova Dumka, Kiev